

Chronicles in Ivory: Estimating the age of narwhals (*Monodon monoceros*) through stochastic modelling of seasonally varying trace elements

Lars R. Nielsen^{1,*}, Tonny B. Thomsen², Benjamin D. Heredia², Mads Peter Heide-Jørgensen³, Susanne Ditlevsen¹, Eva Garde³

¹Department of Mathematical Sciences, University of Copenhagen, Copenhagen, Denmark

²Geological Survey of Denmark and Greenland (GEUS), Department for Mapping and Mineral Resources, Copenhagen, Denmark

³Greenland Institute of Natural Resources, Copenhagen, Denmark

Correspondence*:

Lars Reiter Nielsen
lrn@math.ku.dk

ABSTRACT

Age estimation is an important research topic and many techniques have been developed, each with their own strength and limitations, including manual counting of growth layers in bone, carbon dating and the use of hormonal and biochemical markers, among others. In this study, we apply a novel age-estimation method on trace element signals with seasonal components obtained using Laser Ablation Inductively Coupled Plasma Mass Spectrometry (LA-ICP-MS) on tusks from 15 narwhals. We model tusk growth as a strictly increasing stochastic process that, by hypothesis, tracks the number of elapsed annual cycles. For each tusk, we estimate this process to derive model-based age estimates and compare the results with existing methods. We discuss the assumptions underlying our model and its limitations in the context of age estimation.

Keywords: sclerochronology, stable isotopes, age estimation, time warping, LA-ICP-MS, stochastic process, growth layer

1 INTRODUCTION

Narwhals (*Monodon monoceros*) are renowned for their distinctive spiral tusks similar to that of the mythical unicorns. These tusks, predominantly a male characteristic, emerge early in life from the upper left lip and show continuous growth throughout the narwhal's lifespan (Garde and Heide-Jørgensen, 2022). Within these tusks, Growth Layer Groups (GLGs) form annually (ref). The traditional method for estimating age in toothed whales involves counting the GLGs in the dentin or cementum (ref). However, this approach is subjective, lacks a quantification of uncertainty, and is often challenging due to layer compression, cementum occlusion at the root [(Watt et al., 2020), (Read et al., 2018, p. 13)], or faint visibility. Here, we will apply a stochastic model that take advantage of that these GLGs incorporate elements in varying concentrations. Revealing the elemental composition across such growth layers provides a chronological record of the narwhal's life, thus offering, among other insights, a way to quantify its growth and age

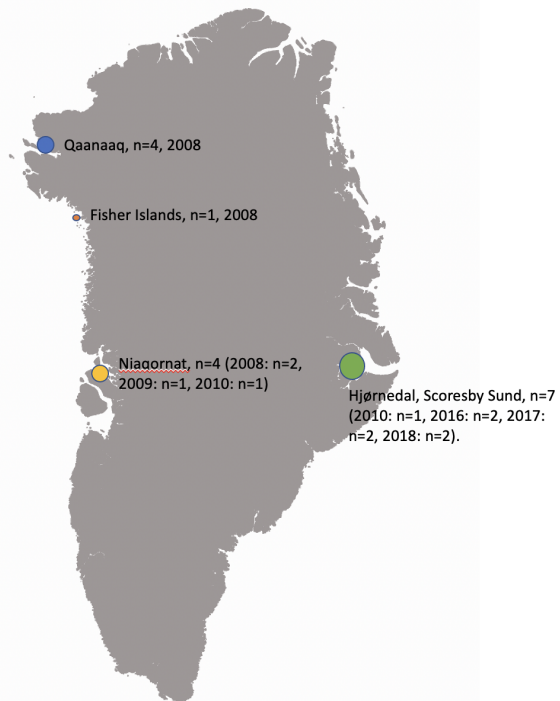


Figure 1A. Locations where whales were captured are highlighted.

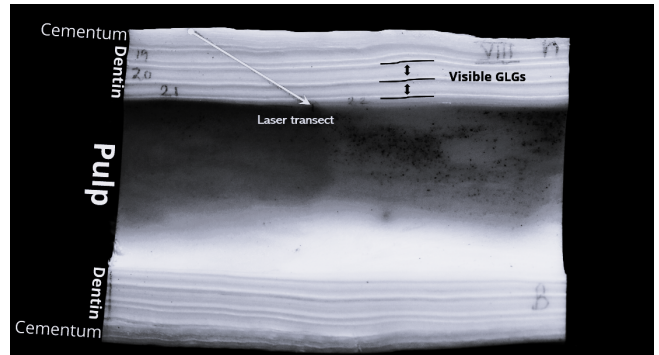


Figure 1B. Red line marks the laser transect used to measure elemental concentrations. Blue lines illustrate visible GLGs. The narwhal tusk has three main parts: the outer cementum (porous and flexible), the dentin (which exhibits growth layers used to estimate age), and the pulp cavity (which contains blood vessels and nerves; note that the pulp has been rinsed in this picture).

Figure 1. (A) Map of Greenland. **(B)** Example of a Narwhal tusk piece analyzed with LA-ICP-MS.

through means of an objective model approach (ref til din egen paper). To unlock the elemental record, we used Laser Ablation Inductively Coupled Mass Spectrometry (LA-ICP-MS), which is a powerful analytical tool that can precisely measure trace elements and isotope ratios in solid materials (ref). Widely used in geological, biological and related fields, this technique allows a detailed analysis of materials ranging from fish otoliths to tree rings (Heimbrand et al., 2020; Fink-Jensen et al., 2021; Smith et al., 2021; Bind et al., 2021; Koch and Günther, 2011). In this study, we used LA-ICP-MS to derive elemental signals with strong seasonal components from 15 narwhal tusks (see Table 1) collected at four different sites in Greenland. Due to the size constraints of the laboratory equipment, we carefully segmented each tusk into multiple tusk pieces, such that each piece covers new growth layers. We then processed the piecewise signals using a novel time-warping model introduced in Nielsen et al. (2024), which incorporates a hidden stochastic process that captures empirically observed variations in growth rate. By first estimating the process for each tusk piece, we reconstructed a continuous growth signal for the entire tusk, enabling us to produce age estimates for all whales. To properly merge the piecewise signals, we also developed a method to account for temporal overlaps between consecutive tusk pieces.

2 MATERIALS AND METHODS

2.1 Data acquisition and LA-ICP-MS

2.1.1 Sample collection, preparation and analytical setup

The narwhal tusks were collected from the Inuit hunt of narwhals during the period from 2008 to 2018. The tusks had been sectioned longitudinally for previous studies. For this study, the tusks were cut into

smaller pieces of < 10 cm in length to fit into the analytical equipment (Figure 1B). Only tusk pieces expected to cover new sets of GLGs were selected. The surface of the tusk half sides was polished, and growth zones of the tusks were determined through reflectance light optical images obtained by a Zeiss desktop microscopy and associated imaging software at Greenland Institute of Natural Resources (GINR). X-ray fluorescence spectrometry (XRF) was used to map the major elemental components of the identified growth layers in the tusk. The elemental abundance obtained through the XRF analyses was used as reference concentration for the succeeding LA-ICP-MS analysis to measure the detailed compositional variations in the tusk expressed as differences in element ratios or absolute abundances.

2.1.2 Microchemical analysis

The trace element composition of the narwhal tusk was measured along a transect running across the growth zones in the direction from the cementum to the pulp cavity, as exemplified in Figure 1B. The analyses were performed at the LA-ICP-MS facility at the Geological Survey of Denmark and Greenland (GEUS). A NWR213 frequency-quintupled Nd:YAG solid state laser system from ESL, employing two-volume cell technology, was coupled to an ELEMENT 2 double-focusing single-collector magnetic sector-field ICP-MS from Thermo-Fisher Scientific. Operating conditions and data acquisition parameters are listed in Tab X in Appendix (TODO: insert table). The general analytical approach and data processing techniques used are described in Serre et al. (2018); Fink-Jensen et al. (2022, 2021); Stounberg et al. (2022) with further details differing from these procedures given herein (in the Supplementary information?).

The LA-ICP-MS analyses are acquired in counts pr. second (cps) for each isotope measured along the transect. To calculate elemental abundances (e.g. $\mu\text{g/g}$) we use a stoichiometrically known internal standard element and an external standard reference matrix (NIST-610 glass) with known element concentrations. For the analyses of the narwhal tusks, Ca was used as the internal standard element due to the tusk's robust calcium-phosphate (hydro-apatite?) structure. The Ca concentration in the tusk was set to 53.789 wt% Ca representing the averaged Ca content obtained by the XRF measurements. Although variations in the Ca content across the transects in the tusk are plausible, it was not the scope here to examine the details in Ca variations across the growth zones. Nevertheless, the Ca signal was qualitatively monitored and assessed throughout each analytical sequences for its stability and robustness for the abundance content calculations. This showed consistent Ca content along the line transects within a few % internal uncertainty, suggesting that it is reasonable to assume a consistent Ca content for the narwhal tusk. Any variation in the abundance of Ca will naturally affect the absolute abundance determinations of the elements measured, whereas it does not affect element ratios determined relative to Ca.

The ICP-MS was optimized for dry plasma conditions through continuous linear ablation of the NIST-610 glass reference material. The signal-to-noise ratios were maximized for isotopes in the entire mass range from Li to U, opting simultaneously for low element-oxide production levels by minimizing the $^{238}\text{U}^{16}\text{O}/^{238}\text{U}$ ratios. Instrumental drift was minimized by following a standard-sample-standard analysis protocol, bracketing single transects with NIST-610 (Jochum et al., 2011) and BHVO-2 glass (Jochum et al., 2016) measurements. The quality of the measurements was furthermore controlled by repeated measurements of known-unknown analyses of the NIST-612 and NIST-614 SRM glasses, yielding typical 2σ accuracies of < 5% deviation for elemental concentrations above 1 $\mu\text{g/g}$. Figure 2 shows the accuracy of the measurements compared to published reference values of the standard reference materials employed in the study, and which shows a general good agreement with the reference values, thus confirming the robustness of the analytical method used to measure the tusks.

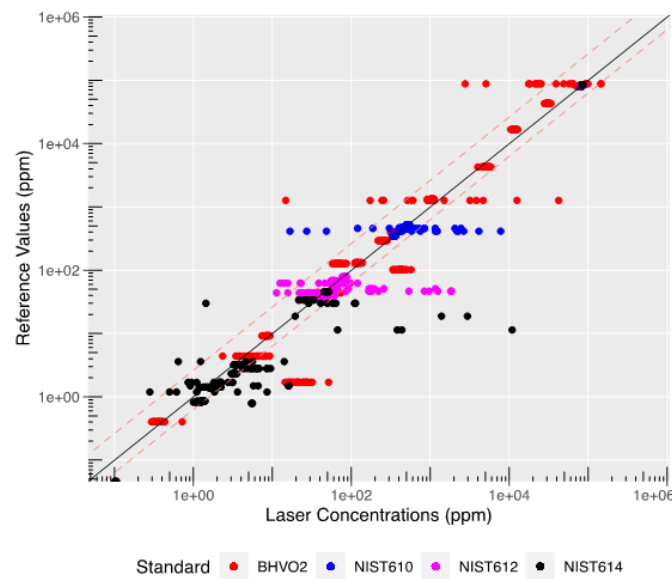


Figure 2. Illustration of the laser measurements against the reference values from Jochum et al. (2011, 2016), measured through 20 sessions. There is a systematic deviation of Pb in the BHVO-2 due to possible Pb-common contribution, although this is not noticeable in the NIST-610, NIST-612 nor NIST-614. High dispersion towards overestimated values of P and K is attributed to a high background at the time the experiments started. Solid black line indicated 1:1 fit, whereas dashed lines indicate a $\pm 10\%$ deviation from the reference values.

Data were acquired from linear transects across tusk pieces using a $40 \mu\text{m}$ spot size, a pulse rate of 10 Hz and a nominal laser fluence of 2-3 J/cm^2 . Total acquisition time for single analyses varied depending of the length of the tusk piece, but included 30 s gas blank measurement followed by laser ablation of the tusk piece and washout for 30 s before the laser moved to the next experiment. Factory-supplied software from Thermo-Fisher Scientific was used for the acquisition of the transient data. Data reduction and determination of concentrations was performed off-line through the software iolite4 (Hellstrom et al., 2008; Smith et al., 2021) using the Trace Elements data reduction scheme.

2.1.3 Omitting cementum and pulp contribution

Material is continuously deposited at the root of narwhal tusks, forming GLGs composed of alternating dark and light bands, which are believed to represent annual cycles, as confirmed across several species (Scheffer and Myrick, 1980) (Perrin et al., 2009, p. 606) (Scheffer and Myrick, 1980; Hohn et al., 2016; Waugh et al., 2018). Dentin GLGs are preferred for age estimation because they are more easily distinguishable compared to cementum (Garde et al., 2012), and we follow this established practice. To mitigate the influence of cementum (and, potentially, pulp) in the LA-ICP-MS signals, we measured the width of the cementum and pulp along the laser transect using a vernier caliper. Based on the laser's movement speed of roughly $4\mu\text{m}$ per second, we then truncated the signal at the corresponding time points. The exact junction between cementum and dentin is hard to observe, and it is difficult to confirm whether the laser traversed the pulp cavity. Consequently and in addition to the caliper measurements, we examined the elemental signals of zinc (Zn) in each tusk piece (see Figure 3A for such a profile), as Zn concentrations are known to be elevated in cementum and pulp regions (Dean et al., 2018; Martin et al., 2007; Clark et al., 2020b). This is illustrated in Figure 3B, which shows the zinc content in one of our tusk pieces, as measured using X-ray fluorescence (XRF) spectroscopy.

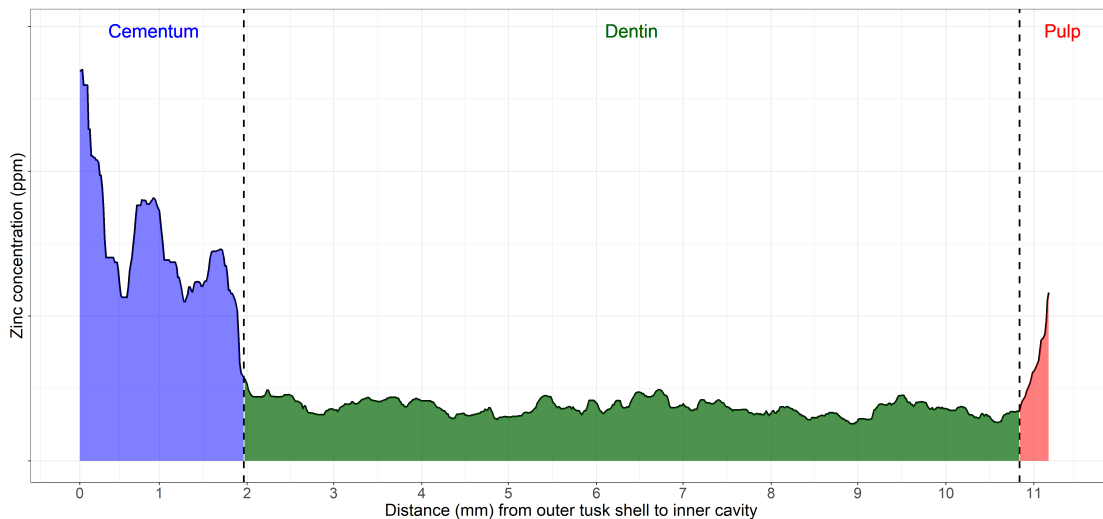


Figure 3A. The blue, green and red area is the presumed region of cementum, dentin and pulp, respectively. Regions of pulp and cementum show elevated zinc levels.

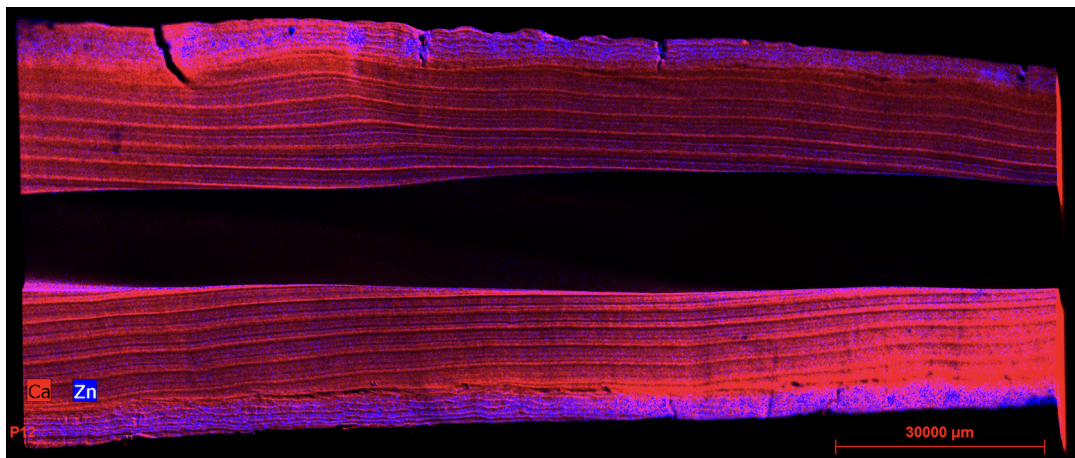


Figure 3B. Zinc concentrations (in blue) in the cementum part of a tusk piece, compared to the calcium levels (in red), more pronounced in the dentin part.

Figure 3. (A) Zinc (^{66}Zn) signal for Tusk 956, piece V. (B) X-ray fluorescence tusk image.

2.2 Elemental compositions with seasonal signatures

LA-ICP-MS was set to acquire 18 elemental signals for each tusk piece across all 15 tusks. Here we focused on strontium (^{88}Sr) and barium (^{137}Ba), since these elements show the most distinct cyclic variations (see Figure 4) assumed to be driven by migration between winter and summer grounds (Ruiz-Sagalés et al., 2024, p. 4) (Heimbrand et al., 2020), thereby providing proxies for age estimation. In addition to the cyclic variations visible in some elements, we observe that the intake is variable between groups of elements. Sometimes, the change is age-related and gradually decreases as we go from early GLGs (near the tip) in the juvenile phase to the prime of the narwhal (near the root). Other times it is more irregular, and linked to intrinsic biological processes or environmental influences. For instance, Ba is observed to be relatively high in the nursing stage of a narwhal's life, possibly due to higher intake of milk (Clark et al., 2020a). For our purpose of age estimation, any trend adds unnecessary complexity, since we

only need a model to capture the dynamics of the repeating cycles. Thus, we start by decomposing the signal, and focus our attention on the cyclic component. The trend components were estimated using local polynomial regression (LOESS) implemented in the statistical program R. This estimation was performed on the signal for the entire tusk, i.e. by combining the signals from each tusk piece in chronological order. The cyclic components were then estimated by subtracting the trend from the signal(s). An example of such a decomposition is shown in Figure 4. The figure also shows that (standardized) Ba and Sr are almost interchangeable. This is highlighted in Figure 5, where we have plotted the trend correlation and cyclic correlation as a 2-dimensional point for each tusk. The figure has four panels, wherein we compare Ba, the element with the most prominent cyclicity, to four other top candidate elements showing visible cycles, namely Sr, Li, Cu and Pb. In the lower right panel, we see that Ba and Sr simultaneously show a strong trend association and phase alignment (cycles occur at equal points in time). For these elements, a spearman correlation test across pooled tusks also showed a highly significant relationship ($p < 2.2 \times 10^{-16}$; Bonferroni adjusted p-value for double testing), with an average (over all tusks) correlation pair of 0.49 and 0.58 for the trend and cycle component, respectively. We chose the spearman correlation coefficient to account for non-linear associations. While Ba and Sr may seem nearly identical, the signal-to-noise ratio can differ significantly within a tusk piece. We therefore used the aggregated signal $^{137}\text{Ba} + ^{88}\text{Sr}$ for the age estimation. We also assumed that all growth layers were present in the tusk pieces that make up an entire tusk, such that when pieced together the signal cover the entire lifespan of the narwhals (except for possible missing tusk tips; see Section 4)

2.3 A time warping model

Let $y_i = y(x_i)$ be the detrended (see section 2.2) elemental concentration of the aggregated signal from Ba and Sr at a distance $x_i = \Delta i$ from the cementum-dentin junction along the laser transect of the tusk piece, where $\Delta = x_i - x_{i-1}$ is the distance between measurements and $i = 1, \dots, n$ with n equal to the number of measurements. The measurement at position x_i then corresponds to the elemental deposition at an unknown time through an increasing function g , $t_i = g(x_i)$, which we denote the growth-time process, since the increase in g from position x_i to position x_{i+1} gives the time passed for the tusk to grow a distance $x_{i+1} - x_i$ along the laser transect. We impose that g is a strictly increasing function with respect to x , which ensures that time never goes backward.

The growth-time process is then defined as the integral of an instantaneous growth process ξ_x (growth rate at time $t_x = g(x)$), which we assume is stochastic due to environmental, seasonal and internal variability in the growth of the tusk. The process ξ_x should then be positive, since the tusk can only grow and not shrink. We assume it varies stochastically around some mean growth rate $\alpha > 0$. We use the so-called square-root (SQR) diffusion, which is a positive stochastic process with governing equation

$$d\xi_x = -\beta(\xi_x - \alpha)dx + \omega\sqrt{\xi_x}dW_x, \quad \xi_0 = 0,$$

with parameters mean (α), rate of adjustment (β) and variance ($\omega^2/(2\beta)$), and W_t is a Wiener process modeling the unknown deviations from the mean as stochastic.

The growth-time process is then defined as $g(x) = \int_0^x \xi_s ds$, so g is also stochastic, and strictly increasing, since $\xi_x > 0$, ensuring non-reversion of time. Whenever ξ_x increases, it indicates a deceleration in the growth of the tusk (since the resulting increase in g indicates that more time has passed for the same amount of dentin growth).

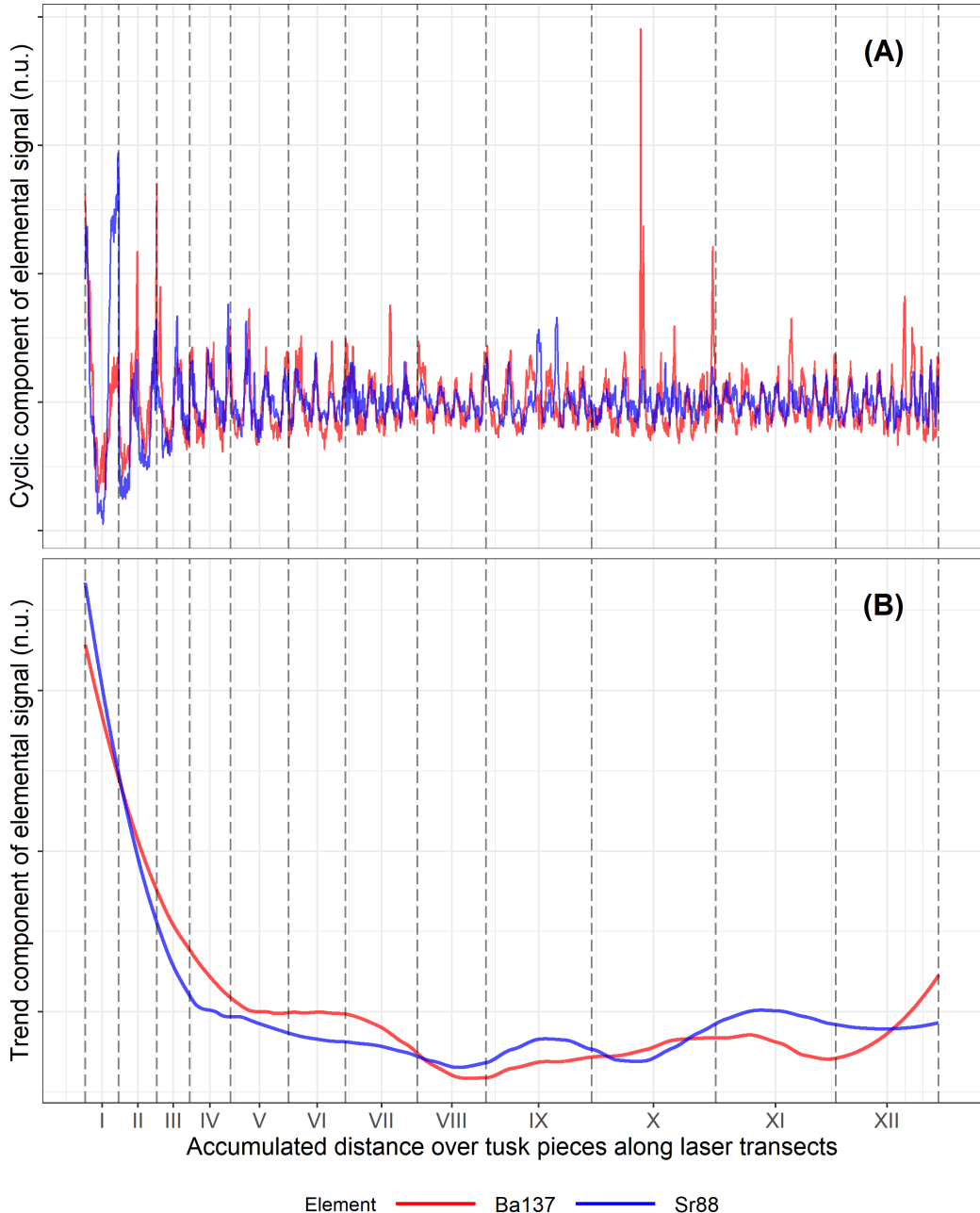


Figure 4. Standardized (no units; n.u.) signals of Ba (red) and Sr (blue), separated into cyclic component (Figure A) and trend component (Figure B) for 12 tusk pieces from tusk 956. Standardization was done by dividing with the signals standard deviation. The trend was then obtained using local polynomial regression, with a span parameter equal to 30% of neighboring points. Vertical dashed lines mark transitions between tusk pieces. For this tusk, the spearman correlation between Ba and Sr is 0.6 and 0.71 for cyclic and trend component, respectively.

We assume the following form for the evolution of the element measurements

$$y_i = \underbrace{A \sin(g(x_i) + b)}_{\text{Annual cycles}} - \underbrace{B(x_i) \cos(2g(x_i) + 2b)}_{\text{Summer/winter differences}} + \epsilon_i, \quad i = 0, 1, \dots, n; x_i = i\Delta; g(0) = 0 \quad (1)$$

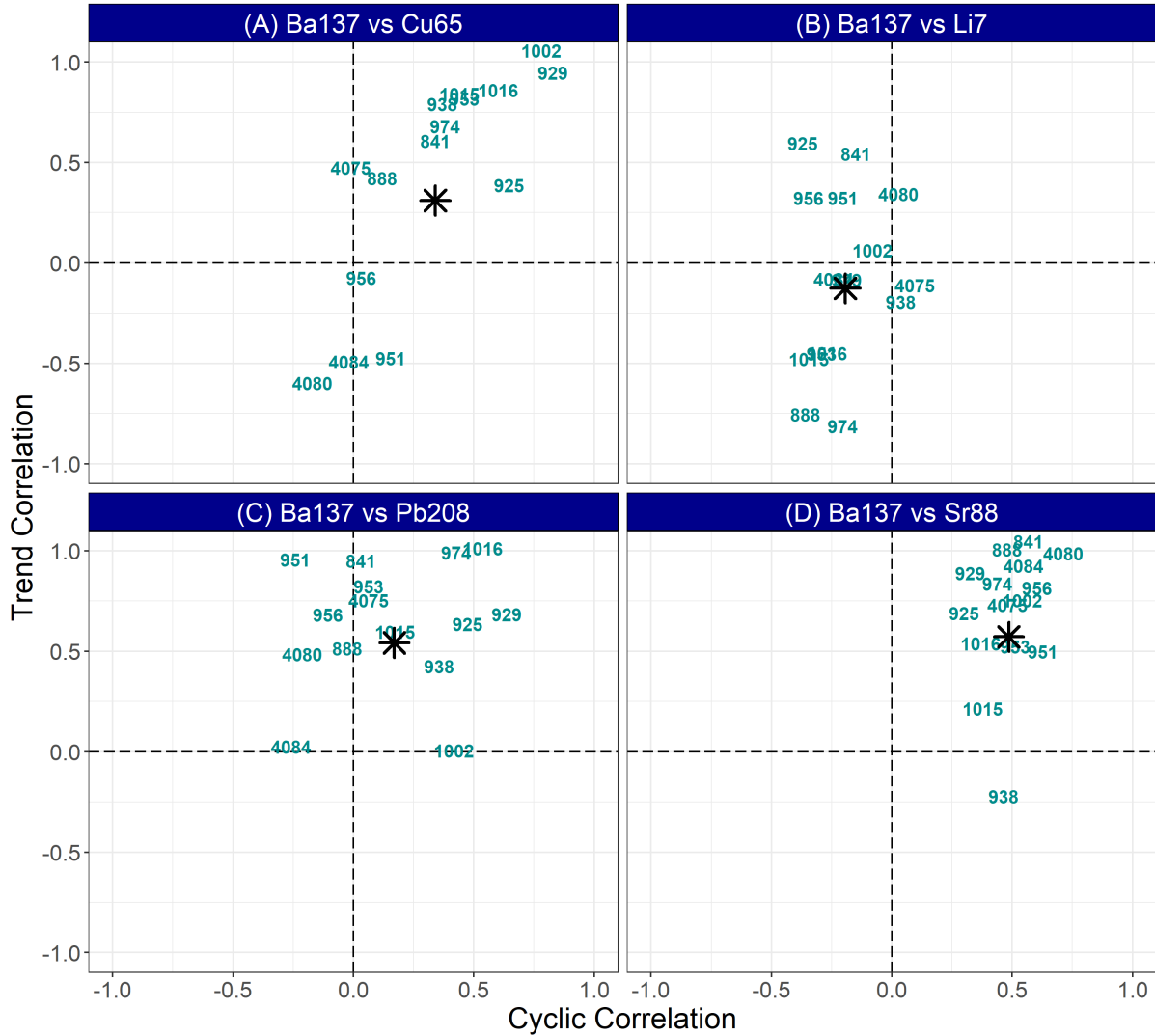


Figure 5. Spearman correlation of Ba against Cu (Figure A), Li (Figure B), Pb (Figure C) and Sr (Figure D) for the trend component and cyclic component for each whale/tusk marked with the number identifier. Black stars are the means (centroids) of the correlations, weighted by the number of measurements within each tusk.

where ϵ_i is assumed independent and normally distributed measurement error with mean 0 and variance σ^2 . The parameter A represents the baseline amplitude of the elemental concentration during summer (or winter), while $B(x)$ modulates this amplitude, accounting for seasonal variations. The offset parameter b determines the point in the season at which the signal begins.

The growth-time process $g(x)$ provides the (current) age in years at any spatial position x_i , through counting the elapsed number of cycles, meaning that:

$$\text{Age}(x_i) = \text{Elapsed number of cycles} = \frac{g(x_i)}{2\pi}, \quad i = 1, \dots, n \quad (2)$$

$$\text{Age of whale} = \text{Age}(x_n) \quad (3)$$

Equation (2) and (3) assume here that $g(x)$ is the growth-time process of the entire tusk, and x_n is the total distance covered across all tusk pieces. The model was fitted to each individual tusk piece of the tusk,

whereafter the growth time processes were concatenated (taking into account possible overlaps; see Section 2.3.1) in chronological order, i.e. from the tip of the tusk to the root segment. Given the year of death (time of capture) $\text{Year}_{\text{Death}}$ of a whale, we then match elemental signal events x_i to an annual timeline as:

$$\text{Year}(x_i) = \text{Year}_{\text{Death}} - (\text{Age}(x_n) - \text{Age}(x_i)), \quad i = 1, \dots, n. \quad (4)$$

Expressing the observations y_i in terms of time coordinates t_i instead of length coordinates x_i , we denote time warping.

The model was fitted using a variant of the Stochastic Approximation Expectation Maximization (SAEM) algorithm (Ditlevsen and Samson, 2014). Residual bootstrapping was used to produce confidence intervals for the age estimate. See Nielsen et al. (2024) or supplementary materials for further details on the model and the estimation method.

2.3.1 Overlapping pieces

When segmenting a narwhal tusk into consecutive tusk pieces, particular attention was paid to ensuring that segmented tusk pieces covered all GLG. However, overlaps between the growth layers of adjacent tusk pieces is expected. To handle this, visual readings of tusk growth layers were done, giving estimates that ranged from 0 to 14, with a median of four overlaps.

If the manual estimate of overlaps between two consecutive tusk pieces was zero, we accepted it without further analysis. If overlaps were identified, we calculated the sum of least squares to determine the most likely overlap between consecutive tusk pieces, guided by the model estimated growth-time process $\hat{g}(x)$, and the estimated phase \hat{b} , from each tusk piece. The procedure can be summarized in four steps:

1. **Identification of annual intervals.** For each tusk piece, we used $\hat{g}(x)$ and \hat{b} to identify the annual intervals, i.e. when a year starts and ends. This amounts to finding all x where $\hat{g}(x) + \hat{b}$ is equal to an odd multiple of $\frac{\pi}{2}$.
2. **Matching and comparing observations between consecutive tusk pieces:** We aligned the observations y_i from each annual interval of the first tusk piece with the observations of the first annual interval of the adjacent tusk piece. This was done on the time warped scale, i.e. by expressing observations in terms of time, $y_i = y(t_i)$, such that measurements on one tusk piece were matched to measurements on the other tusk piece believed to be deposited at the same time. To ensure compatibility, we adjusted the resolution of the first tusk piece intervals, through interpolation or subsampling, to match the resolution of the annual interval of the second tusk piece. We standardized the observations to account for variations in scale. This was done by subtracting the signal mean and dividing by the signal standard deviation. Finally, we computed the mean of the least squares difference between observations from each interval of the first tusk piece and observations from the first interval of the second tusk piece.
3. **Including unfinished year.** Each tusk piece also had an unfinished year at the end of the signal. This interval (start of year to end of signal) was also included, and handled similar as in step 2, except that it was compared to the same annual fraction of the interval from the following tusk piece.
4. **Selecting the Best Match.** We chose the interval from the first tusk piece, which had the smallest difference, with the interval of the second tusk piece, as our best estimate of an overlapping year. The overlapping data, along with remaining data beyond the boundary of that interval, was subsequently removed from the first tusk piece.

If only one annual peak was found in the first tusk piece, we then assumed there was no overlap. Similarly, if the second tusk piece had just one peak, we also assumed no overlap. The entire procedure is visualized in Figure 6.

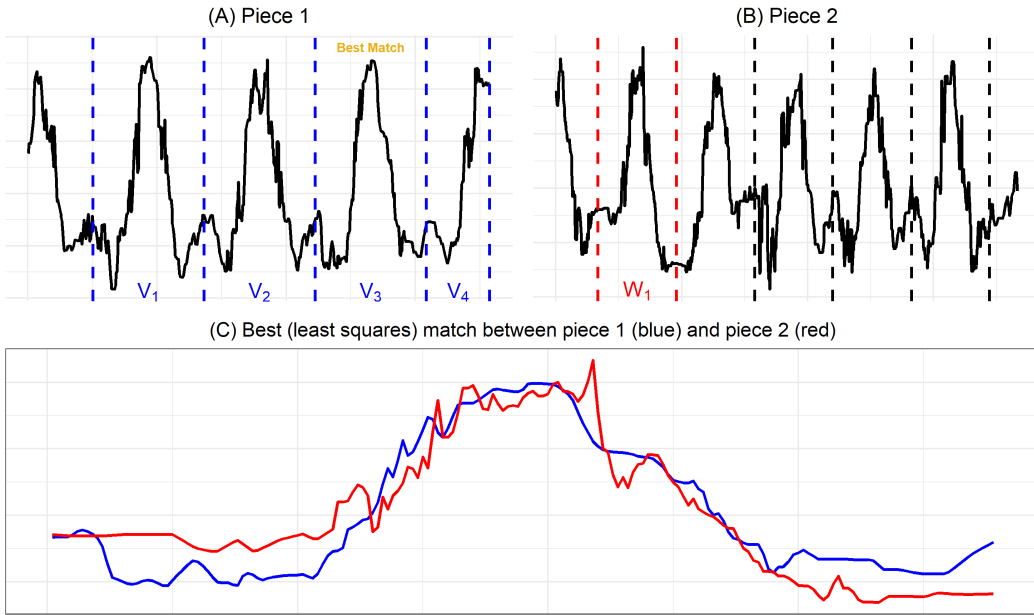


Figure 6. Illustration of the least squares estimation for overlapping growth layers on tusk 956, between tusk pieces VIII and IX. (A) Time warped signal of piece VIII. The signal traverse 3 years (V_1 , V_2 and V_3) and we extend with a unfinished year V_4 . (B) Time-warped signal of piece IX with the first year (W_1) marked by red dashed lines, and other years (unused) indicated by black horizontal lines. (C) The best overlap (in the least squares sense) occurs between V_3 and W_1 . Each signal has been standardized prior to comparison. The method estimates an overlap of 1.57 years, compared to a manual reading of 1 year.

3 RESULTS

Figure 7 shows the fitted signal alongside the stochastic model components and time warping, for one of the tusk pieces. As we traverse the tusk piece transect, the growth-time process $g(x)$ slightly steepens, indicating a decline in growth. This is clearer in the bottom panel, where annual intervals contract. On the time-warped scale (in purple), the signal is stretched to ensure uniform annual intervals.

In Figure 8 we visualize the likelihood of narwhal ages for each tusk, as predicted by our model described in 2.3. The x -axis displays the age, and the blue density can be interpreted as the model's confidence in that age; when the density is narrow and high there is little uncertainty to the age-estimate, whereas when low and wide, there is much more uncertainty. The mean age estimate (in red) along with the manual reading of GLGs (in green) is also marked. For the majority of the tusks, the GLG reading is in reasonable agreement with the model predictions, but there are also exceptions, such as tusk 1015, 929 and 925. The panels of Figure 8 are sorted (top to bottom) according to the estimated mean age, and we also inserted drawings of the tusks in each panel to simultaneously inspect how age estimates relates to length of tusk. The figure indicates a general trend of longer tusks in older narwhals, yet substantial variability is observed. Some older individuals have relatively short tusks, while certain younger whales display larger ones, indicating that other factors beside age influence the tusk size. For some of the tusks, uncertainty estimates are narrow, which means the bootstrap created signal replicates with low variability. When signals do not show clear

cycles nor conform to the model specification (equation (1)), for example due to the presence of secondary cycles (see section 4), we expect to see more variability. In contrast, for optimal signals, such as those seen in tusk 956 (see Figure 5), we obtain a more precise estimate.

Table 1 summarizes the estimated overlaps, including both visual assessments and algorithmic estimates from the procedure described in section 2.3.1. These estimates do in general agree, except for a few cases, such as tusk 929, 925 and 1015 where the difference between the number of overlaps for the visual reading and the algorithm is 5, 4 and 5 respectively. As noted above, tusk 929 and 1015 also yielded age estimates which differed substantially from the GLG reading in Figure 8, thus this could be due to the disagreement in overlap.

In Table 1 we present the estimated ages using equation 4, along with the a 95% bootstrap confidence interval. These ages are compared to visual readings of the GLGs and other previous attempted age estimation techniques applied to the same sample of narwhals. As was also hinted at in Figure 8, we see that nearly all measured GLGs are in agreement with the estimated age, using the assumption that one year corresponds to one GLG. The exceptions being 929 and 1015.

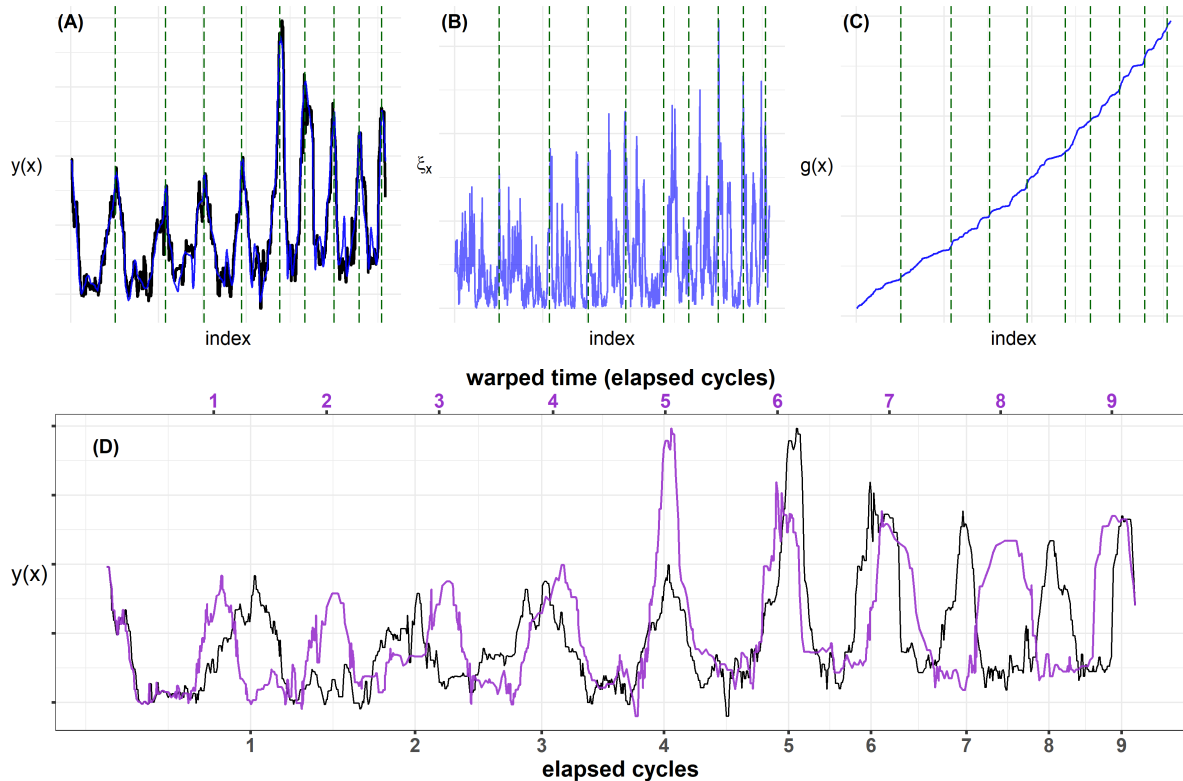


Figure 7. Model figures from tusk 956, piece XII. (A) Raw signal (black) and fitted signal (blue). (B) Square-root process ξ_x (blue). (C) Growth-time process (blue). In all plots, estimated years (equation (2)) are marked as dashed green lines. (D) Time warped signal (purple) and the original signal (black). Years are shown both on the time-warped scale (equidistant) and on the original scale.

4 DISCUSSION

There exist a variety of age estimation techniques (Watt et al., 2020; Garde et al., 2012; Barratclough et al., 2023), each with their own strength and limitations. In this study, we used LA-ICP-MS, a modern and

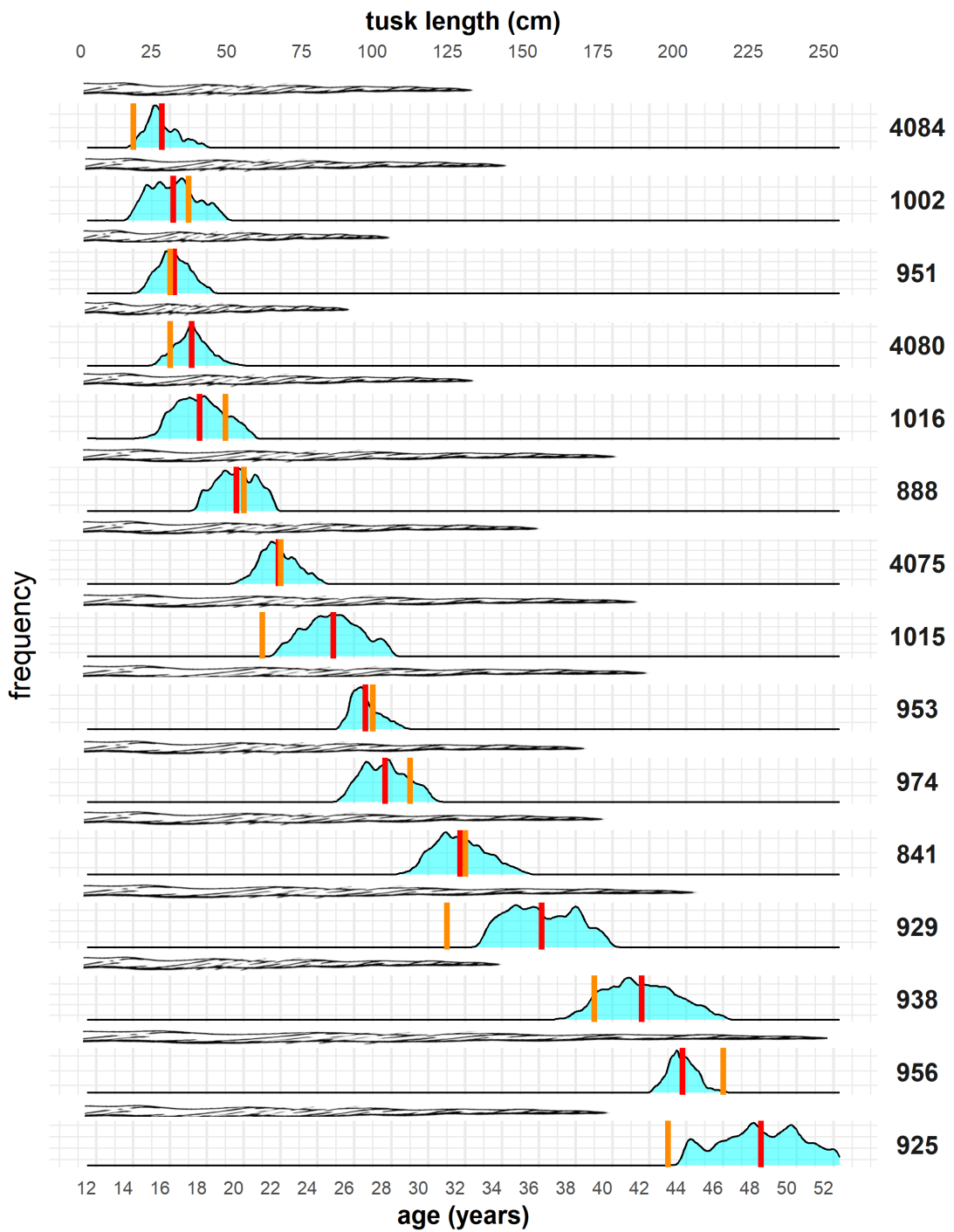


Figure 8. Age density plots and tusk length for all 15 tusks. For each tusk, we fitted the time warping model (section 2.3) to data from each separate tusk piece. Residual bootstrapping was then performed on the fitted signal for each tusk piece to generate $M = 100$ bootstrapped versions of the growth-time process $g(x)$. A single bootstrapped version was randomly selected for each tusk piece, and the selected processes were then concatenated to form a complete growth-time process for the entire tusk. This procedure was repeated 100.000 times, generating 100.000 complete growth-time processes for each tusk, hence a 100.000 age estimates using equation (3). The densities of these estimates are shown in blue. The average age estimate is shown as a red vertical line. The manual GLG reading of each tusk is shown as a orange vertical line. The length of the tusks are visualized with animations at the top of each panel. The relevant length axis is positioned at the top.

versatile technique, to obtain precise elemental signals in the tusks of narwhals, which can be linked to chronological measurements, correlating with the seasonal cycles observed in the species. Using a novel time warping model that captures the dynamics of the seasonal signals, we translated spatial locations on tusk cross-sections into annual events, providing new and refined age estimates.

Age estimation based on dentin GLGs assumes the annual deposition of growth layers (Scheffer and Myrick, 1980). However, several factors complicate this estimation process. First, natural wear may remove the tip of the tusk, including the neonatal line that marks the transition from prenatal to postnatal growth. Such attrition was observed for tusk 4076 and 956. For tusk 953 the tip was intact, but worn. Additionally, cementum occlusion in the postnatal stage can obscure the visibility of GLGs [(Watt et al., 2020), (Read et al., 2018, p. 13)], leading to a potential underestimation of the number of growth layers. The process of segmenting the tusk for use in the LA-ICP-MS laboratory also carries the risk of either double-counting certain GLGs or missing intermediate layers, although the latter is considered unlikely. These factors introduce both negative and positive bias to the age estimate expressed as:

$$\text{Age} = \text{Observed GLGs} + \text{Missing GLGs} - \text{Overlapping GLGs}. \quad (5)$$

"Missing GLGs" refers to those that were present in the retrieved tusk, but excluded in the tusk segmentation (we expect none), as well as GLGs obscured by cementum or the neonatal line. In this study, we have focused on estimating the observed and overlapping GLGs, while omitting the contribution of missing GLGs. It is important to note that sub-annual layers (or accessory layers), likely associated with life-history events (Read et al., 2018), are occasionally embedded within the primary growth layers. These sporadic occurrences can risk being misidentified as GLGs, and potentially appear as secondary cycles in the elemental signals, thereby inducing uncertainty to the final age estimate. We consider these issues to be ubiquitous in relation to GLG-based age estimation, underscoring the intrinsic challenges posed by biological complexity and environmental influences rather than methodological shortcomings.

Lars: Tables inserted at END of manuscript. Journal requirement. Also: max 15 figures (Figures in minipage counts as one).

Benjamin: Conclusion section is missing. I have been throughout the text and there have been some typos and grammatical things that I have been correcting. Some statements read ambiguous and they might be sharpen though the main body is looking great. Would the significance test and multi-test correction be added later? I will try to send you asap a the table with laser info and mass spec conditions. I recommend to place all that, together with graph 2 in supplementary section. Please let me know if anything else. BEHE@geus.dk

CONFLICT OF INTEREST STATEMENT

The authors confirm that the research was conducted in the absence of any commercial or financial relationships that could be construed as a potential conflict of interest.

AUTHOR CONTRIBUTIONS

TODO: All authors fill in with contribution.

LRN: Methodology, Formal analysis, Software, Visualization, Writing – original draft.

Please see here for full authorship criteria.

Tusk ID	4080	4084	4075	4076	841	951	953	888	956	974	925	929	938	1002	1015	1016
Sex	F	F	F	NA	M	M	M	M	M	M	M	F	M	M	M	M
Year	2008	2008	2008	NA	2008	2008	2008	2009	2010	2010	2016	2016	2017	2017	2018	2018
Region	NGL	NGL	NGL	NA	NGL	WGL	WGL	WGL	EGL							
Tusk length (cm)	92	130	164	NA	179	109	194	181	255	173	181	210	144	145	191	134
Neonatal	Yes	Yes	Yes	NA	Yes	Yes	Yes	Yes	(Yes)	Yes	-	-	No	Yes	-	-
Tusk tip	Yes	Yes	Yes	NA	Yes	Yes	Yes	Yes	Yes	Yes	-	-	No	Yes	-	-
Tusk base	No	No	Yes	NA	Yes	Yes	No	No	Yes	Yes	-	-	Yes	Yes	-	-
Overlap visual reading	0	2	0	NA	0	0	4	0	7	1	14	11	6	5	9	6
Overlap least squares	0	1	0	NA	0	0	4	0	9	1	10	6	3	5	4	7
TW age estimate [lower, upper]	17 [15-19]	16 [14-18]	22 [20-24]	NA	32 [29-35]	16 [15-18]	28 [26-30]	21 [19-23]	44 [42-46]	28 [25-30]	48 [44-42]	36 [33-40]	42 [39-46]	16 [14-19]	25 [22-28]	18 [15-20]
GLG visual reading	16	14	22	NA	32	16	27	20	46	29	43	31	39	17	21	19
AAR age estimate	NA	NA	NA	NA	NA	NA	NA	NA	NA	NA	NA	NA	NA	NA	NA	NA

Table 1. The tusk sample used in this study. The table includes information about gender (F = female, M = male), and the year and region where the narwhal was captured (NGL = North Greenland, WGL = West Greenland and EGL = East Greenland). The tusk length was measured after extraction from the cranium. For some of the tusks, the neonatal line, tip of the tusk, base of the tusk or any combination of these was missing. If present, we record it as yes, otherwise no. Few tusks had missing information. The table also includes the estimated overlaps from visual readings and least squares, as well as the estimated age based on the time warping (TW) model, including bootstrap 95% confidence intervals. Estimated GLGs from visual reading and estimated age from the Aspartic Acid Razemization (AAR) technique is also included.

FUNDING

TODO: Fill out.

ACKNOWLEDGMENTS

We would like to thank...

SUPPLEMENTAL DATA

TODO: Include anything in supplementary? Code, datasets, LA-ICP-MS figures, other figures? Supplementary Material should be uploaded separately on submission, if there are Supplementary Figures, please include the caption in the same file as the figure. LaTeX Supplementary Material templates can be found in the Frontiers LaTeX folder.

DATA AVAILABILITY STATEMENT

TODO: Upload on GITHUB or ERDA? The datasets [GENERATED/ANALYZED] for this study can be found in the [NAME OF REPOSITORY] [LINK].

REFERENCES

- Barratclough, A., McFee, W. E., Stolen, M., Hohn, A. A., Lovewell, G. N., Gomez, F. M., et al. (2023). How to estimate age of old bottlenose dolphins (*tursiops truncatus*); by tooth or pectoral flipper? *Frontiers in Marine Science* 10, 1135521

- Binda, G., Di Iorio, A., and Monticelli, D. (2021). The what, how, why, and when of dendrochemistry:(paleo) environmental information from the chemical analysis of tree rings. *Science of the Total Environment* 758, 143672
- Clark, C. T., Horstmann, L., and Misarti, N. (2020a). Evaluating tooth strontium and barium as indicators of weaning age in pacific walruses. *Methods in Ecology and Evolution* 11, 1626–1638. doi:<https://doi.org/10.1111/2041-210X.13482>
- Clark, C. T., Horstmann, L., and Misarti, N. (2020b). Zinc concentrations in teeth of female walruses reflect the onset of reproductive maturity. *Conservation Physiology* 8, coaa029
- Dean, C., Le Cabec, A., Spiers, K., Zhang, Y., and Garrevoet, J. (2018). Incremental distribution of strontium and zinc in great ape and fossil hominin cementum using synchrotron x-ray fluorescence mapping. *Journal of the Royal Society Interface* 15, 20170626
- Ditlevsen, S. and Samson, A. (2014). Estimation in the partially observed stochastic Morris–Lecar neuronal model with particle filter and stochastic approximation methods. *The Annals of Applied Statistics* 8, 674 – 702. doi:[10.1214/14-AOAS729](https://doi.org/10.1214/14-AOAS729)
- Fink-Jensen, P., Hüsse, K., Thomsen, T. B., Serre, S. H., Søndergaard, J., and Jansen, T. (2022). Lifetime residency of capelin (*mallotus villosus*) in west greenland revealed by temporal patterns in otolith microchemistry. *Fisheries Research* 247, 106172
- Fink-Jensen, P., Jansen, T., Thomsen, T. B., Serre, S. H., and Hüsse, K. (2021). Marine chemistry variation along greenland’s coastline indicated by chemical fingerprints in capelin (*mallotus villosus*) otoliths. *Fisheries Research* 236, 105839
- Garde, E. and Heide-Jørgensen, M. P. (2022). Tusk anomalies in narwhals (*monodon monoceros*) from greenland. *Polar Research* 41
- Garde, E., Peter Heide-Jørgensen, M., Ditlevsen, S., and Hansen, S. H. (2012). Aspartic acid racemization rate in narwhal (*monodon monoceros*) eye lens nuclei estimated by counting of growth layers in tusks. *Polar Research* 31, 15865
- Heimbrand, Y., Limburg, K. E., Hüsse, K., Casini, M., Sjöberg, R., Palmén Bratt, A.-M., et al. (2020). Seeking the true time: Exploring otolith chemistry as an age-determination tool. *Journal of fish biology* 97, 552–565
- Hellstrom, J., Paton, C., Woodhead, J., Herget, J., et al. (2008). Iolite: software for spatially resolved la-(quad and mc) icpms analysis. *Mineralogical Association of Canada short course series* 40, 343–348
- Hohn, A. A., Lockyer, C. H., and Acquarone, M. (2016). Report of the workshop on age estimation in monodontids. *NAMMCO* , 68
- Jochum, K. P., Weis, U., Schwager, B., Stoll, B., Wilson, S. A., Haug, G. H., et al. (2016). Reference values following iso guidelines for frequently requested rock reference materials. *Geostandards and Geoanalytical Research* 40, 333–350
- Jochum, K. P., Weis, U., Stoll, B., Kuzmin, D., Yang, Q., Raczek, I., et al. (2011). Determination of reference values for nist srm 610–617 glasses following iso guidelines. *Geostandards and Geoanalytical Research* 35, 397–429
- Koch, J. and Günther, D. (2011). Review of the state-of-the-art of laser ablation inductively coupled plasma mass spectrometry. *Applied Spectroscopy* 65, 155A–162A
- Martin, R. R., Naftel, S. J., Nelson, A. J., and Iii, W. D. S. (2007). Comparison of the distributions of bromine, lead, and zinc in tooth and bone from an ancient peruvian burial site by x-ray fluorescence. *Canadian Journal of Chemistry* 85, 831–836
- Nielsen, L. R., Heide-Jørgensen, M. P., Garde, E., Samson, A., and Ditlevsen, S. (2024). A time warping model for seasonal data with application to age estimation from narwhal tusks. *arXiv.org* , 2410.05843

- Perrin, W. F., Würsig, B., and Thewissen, J. G. M. (2009). *Encyclopedia of marine mammals* (Academic Press)
- Read, F. L., Hohn, A. A., and Lockyer, C. H. (2018). A review of age estimation methods in marine mammals with special reference to monodontids
- Ruiz-Sagalés, M., García-Vernet, R., Sanchez-Espigares, J., Halldórsson, S. D., Chosson, V., Sigurðsson, G. M., et al. (2024). Baleen stable isotopes reveal climate-driven behavioural shifts in north atlantic fin whales. *Science of the Total Environment* 955, 177164
- Scheffer, V. B. and Myrick, A. (1980). A review of studies to 1970 of growth layers in the teeth of marine mammals. *Rep. Int. Whal. Commn* 3, 51–63
- Serre, S. H., Nielsen, K. E., Fink-Jensen, P., Thomsen, T. B., and Hüssy, K. (2018). Analysis of cod otolith microchemistry by continuous line transects using la-icp-ms. *GEUS Bulletin* 41, 91–94
- Smith, T. M., Cook, L., Dirks, W., Green, D. R., and Austin, C. (2021). Teeth reveal juvenile diet, health and neurotoxicant exposure retrospectively: What biological rhythms and chemical records tell us. *BioEssays* 43, 2000298
- Stounberg, J., Thomsen, T. B., Heredia, B. D., and Hüssy, K. (2022). Eyes and ears: A comparative approach linking the chemical composition of cod otoliths and eye lenses. *Journal of Fish Biology* 101, 985–995
- Watt, C. A., Stewart, B. E., Loseto, L., Halldorson, T., and Ferguson, S. H. (2020). Estimating narwhal (*monodon monoceros*) age using tooth layers and aspartic acid racemization of eye lens nuclei. *Marine Mammal Science* 36, 103–115. doi:<https://doi.org/10.1111/mms.12623>
- Waugh, D. A., Suydam, R. S., Ortiz, J. D., and Thewissen, J. (2018). Validation of growth layer group (glg) depositional rate using daily incremental growth lines in the dentin of beluga (*delphinapterus leucas* (pallas, 1776)) teeth. *PLoS One* 13, e0190498